Journal of Molecular Liquids 229 (2017) 339–345

Contents lists available at ScienceDirect

Journal of Molecular Liquids

journal homepage: www.elsevier.com/locate/molliq

On boundary layer nano-ferroliquid flow under the influence of low oscillating stretchable rotating disk

R. Ellahi [a,b,*], M.H. Tariq [b], M. Hassan [c], K. Vafai [a]

[a] Department of Mechanical Engineering, Bourns Hall, University of California Riverside, USA
[b] Department of Mathematics & Statistics, FBAS, IIUI, H-10 Sector, Islamabad, Pakistan
[c] Department of Mathematics, Faculty of Sciences, HITEC University, Taxila Cantt, Pakistan

ARTICLE INFO

Article history:
Received 4 December 2016
Received in revised form 14 December 2016
Accepted 19 December 2016
Available online 22 December 2016

Keywords:
Ferroliquid
Magnetic field
Low oscillation
Rotating disk
Ham

ABSTRACT

A new model is here proposed to investigate the effects of nano-ferroliquid under the influence of low oscillating over stretchable rotating disk. The basic governing equations are formulated under the effects of magnetic field. The resulting system of partial differential equations is first reduced in non-dimensional form by using proper transformations and then reduced coupled system of differential equations is solved analytically by means of homotopy analysis method (HAM). The physical interpretation of velocity and temperature towards different emerging parameters such as particle concentration and effective magnetization parameter are discussed graphically. The physical parameters such as shear stress at wall, heat transfer rate through wall, boundary layer thickness and volume flow rate in axial direction are also presented in tabular form. Finally a comparison with the existing literature is made as a limiting case of the reported problem and found in good agreement.

1. Introduction

The magnetic field can serve as an effective intends to control magnetic liquid suspension of counterfeit magnetic particles of ferromagnetic materials. Suspensions of these materials in a carrier liquid explored the prospective for a new research field called ferrohydrodynamics [1,2]. Numerous types of magnetic liquids arise with ferrohydrodynamics, the principal type is a colloidal ferroliquid [3,4]. A colloid is a suspension of nano-sized particles of Fe_3O_4 or $\gamma - Fe_3O_4$ etc. in a liquid medium that settles out gradually. However, a true ferroliquid does not settle out. Mostly, ferroliquids are contained small (3–15 nm diameter) particles of solid magnetite coated by molecular nanolayer of a dispersant and suspended in a base liquid. A typical ferroliquid contains approximately 10 particles per cubic meter. Due to vast range of applications of nanoparticles in industrial liquids, it has gained considerable attention of researchers and engineers [5–15] in recent past. A great exertion has been done by researchers for those liquids which do not endure strong variations in viscosity influenced by an electronically well-behaved signal. Consequently, to design a proper magnetic liquid, it is important part to have information about magnetic viscous behavior on liquid [16]. Such types of liquids which have controllable viscosity are mostly utilized in magnetically controlled damping systems. Thus, Magneto viscous impact on magnetic liquids also plays an important role in other applications. Usually, there are two situations canned been arising due to direction of applied magnetic field. When the vorticity of liquid and direction of field are collinear, then no changes occur in viscosity of the liquid. This is happen due to co-linearity of magnetic moment of the particles in the direction of vorticity. However in the other case, if magnetic field is applied in opposite direction of vorticity, the magnetic field will attempt to adjust the magnetic moment towards the direction of field course while the liquid apply a forced round the particles through the stream stabs to disturb magnetic field alliance as well as magnetic moment. This increases the flow resistance and thus the liquid exhibits finer viscosity. In this situation, extra dissipation is manifested as rotational viscosity. So, the applied magnetic torque is combination of rotational viscidness and viscous force that depends on the strength of magnetic field as well as on the direction of the magnetic field in respect to the flow [17,18].

The study of ferroliquid in rotation is another exciting field for researchers. Ferroliquid are famous to show atypical appearances when they are imported on set of rotation on thermo convective. Das Gupta and Gupta [19] investigated thermal convective rotating flow of ferroliquid which layer heated uniformly from bottom. Further, Vaidyanathan et al., [20] introduced the effect of magnetic field dependent viscosity on ferroconvection in a rotating system. In the presence and absence of the effects of rotation and magnetic field dependent viscosity on ferroconvection has been investigated by Ramanathan and Suresh [21]. Ram and Sharma [22] reported the heat transfer rate under magnetization and rotational effects. They calculated that viscosity in consequences of magnetization does not effective to improve heat

* Corresponding author at: Department of Mechanical Engineering, Bourns Hall, University of California Riverside, USA.
E-mail addresses: rellahi@engr.ucr.edu, rahmatellahi@yahoo.com (R. Ellahi).

http://dx.doi.org/10.1016/j.molliq.2016.12.073
0167-7322/

transfer rate as compare to without magnetization. Ram et al. [23] have examined the magneto-viscous effects which are generated by low oscillating magnetic field on nano-ferroliquid over rotating disk.

In the existing literature, there is still no investigation is available which describe the influence of magneto viscous effect under low oscillating magnetic together with heat and mass transfer over rotating disk. This effort is devoted to fill this gap. Magnetic material Fe_3O_4 as nanoparticles and water as a conventional charring liquid are taken into account. Here, the emphasis is also to study that how rotational viscosity occurs in motion of a ferroliquid in order to see its effects on the velocity and temperature profiles. Additionally, for engineering interest, the results for wall shear stress, heat transfers rate at wall, boundary layer displacement, angle of rotation and flow rate under the low oscillating magnetic field and different concentration of particles are computed. After introduction, this paper is arranged in the following fashion. Section 2 contains formulation of the problem. In Section 3 solutions of the problems are presented by using homotopy analysis method which is particularly suitable for nonlinear problems [24–27]. Results and discussion are given in Section 4. Finally Section 5 summaries the concluding remarks.

2. Formulation of the problem

2.1. Physical model

Consider the axially symmetric laminar and non-conducting flow of an incompressible nano-Ferroliquid past a stretchable rotating disk. The disk has stretching speed $\Omega_v r/1-\beta t$ which is proportional to the radius r having angular velocity $\alpha\Omega_v r/1-\beta t$ as shown in Fig. 1.

2.2. Governing equations

The basic governing equations such as containing continuity, motion, temperature, magnetization and rotational are

$$\nabla.\mathbf{V}=0, \tag{1}$$

$$\rho_{nf}\frac{d\mathbf{V}}{dt}=-\nabla p+\mu_{nf}\nabla^2\mathbf{V}+\mu_0(\boldsymbol{M}.\nabla)\boldsymbol{H}+\frac{1}{2\tau_s}\nabla\times(\omega_\rho-\boldsymbol{\Omega}), \tag{2}$$

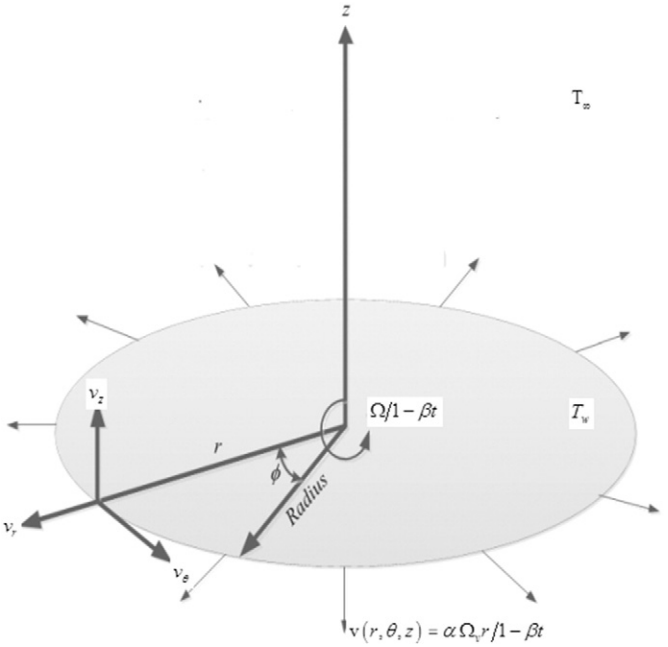

Fig. 1. Geometry of the problem.

$$(\rho C_p)_{nf}\frac{dT}{dt}=k_{nf}\nabla^2T, \tag{3}$$

$$\frac{d\boldsymbol{M}}{dt}=\omega_\rho\times\boldsymbol{M}-\frac{1}{\tau_B}(\boldsymbol{M}-\boldsymbol{M}_0), \tag{4}$$

$$\boldsymbol{I}\frac{d\omega_\rho}{dt}=\boldsymbol{M}\times\boldsymbol{H}-\frac{1}{\tau_S}(\omega_\rho-\boldsymbol{\Omega}). \tag{5}$$

In above equations, $\mathbf{V}=(v_r,v_\theta,v_z)$ is velocity, T is temperature, $\boldsymbol{M}$ is magnetization of the liquid, $\boldsymbol{H}$ is strength magnetic field, τ_s is Relaxation time parameter, τ_B is Brownian relaxation time, μ_0 is permeability of free space, $\boldsymbol{I}$ is sum of moments of inertia of the particles per unit volume, ω_ρ is internal angular momentum due to the self-rotation of particles and $\boldsymbol{\Omega}$ is the vorticity of the flow. The complete set of equations also includes the Maxwell's equations

$$\nabla\times\boldsymbol{H}=0,\nabla.(\boldsymbol{H}+4\pi\boldsymbol{M})=0. \tag{6}$$

The magnetization of the liquid $\boldsymbol{M}$ with the relation of strength magnetic field $\boldsymbol{H}$ is given as

$$\boldsymbol{M}=\boldsymbol{M}_S\left(\coth\xi-\frac{1}{\xi}\right), \tag{7}$$

here, $\boldsymbol{M}_S=\Phi\boldsymbol{M}_0$ is the saturation magnetization in the liquid, which is defined as produce of the volume concentration Φ of the magnetic component and instantaneous magnetization $\boldsymbol{M}_0$ [28,29]. At $\tau_B=0$, the instantaneous equilibrium magnetization $\boldsymbol{M}_0$ is obtained as

$$\boldsymbol{M}_0=nmL(\xi)\frac{\boldsymbol{H}}{H},\xi=\frac{mH}{kT},L(\xi)=\mathrm{Coth}\xi-\xi^{-1}, \tag{8}$$

where ξ is the Langevin parameter, $L(\xi)$ is the Langevin function, k is the Boltzmann constant and n and m are the number of particle and the magnetic moment. Since, τ_s is small, the inertial term is negligible in comparison with relaxation term i.e., $\boldsymbol{I}\frac{d\omega_\rho}{dt}\ll\boldsymbol{I}\frac{\omega_\rho}{\tau_s}$, therefore, Eq. (5) can be written by way of

$$\omega_\rho=\boldsymbol{\Omega}+\frac{\tau_s}{\boldsymbol{I}}(\boldsymbol{M}\times\boldsymbol{H}). \tag{9}$$

Now, Eqs. (2) and (4) in view of Eq. (9) can be written as

$$\rho_{nf}\frac{d\mathbf{V}}{dt}=-\nabla p+(\boldsymbol{M}.\nabla)\boldsymbol{H}+\mu_{nf}\nabla^2\mathbf{V}+\frac{1}{2}\nabla\times(\boldsymbol{M}\times\boldsymbol{H}), \tag{10}$$

$$\frac{d\boldsymbol{M}}{dt}=\boldsymbol{\Omega}\times\boldsymbol{M}-\frac{1}{\tau_B}(\boldsymbol{M}-\boldsymbol{M}_0)+\frac{\tau_s}{I}\boldsymbol{M}\times(\boldsymbol{M}\times\boldsymbol{H}). \tag{11}$$

where $\boldsymbol{M}\times\boldsymbol{H}$is magnetic torques. When both torques; magnetic and viscous will be in equilibrium, then interference of the particle rotation is obtained as

$$\boldsymbol{M}\times\boldsymbol{H}=-6\mu_{nf}\phi(\boldsymbol{\Omega}-\omega_\rho) \tag{12}$$

and

$$\boldsymbol{M}=\frac{\phi\boldsymbol{M}_sL(\boldsymbol{\xi}_e)\boldsymbol{\xi}_e}{\boldsymbol{\xi}}. \tag{13}$$

In which ϕ denotes the volume fraction and effective magnetic field parameter is denoted by $\boldsymbol{\xi}_e$. In the existence of slow oscillating magnetic field Eq. (11) can be written as [30–32]

$$\frac{d}{dt}\left(L_e\frac{\boldsymbol{\xi}_e}{\boldsymbol{\xi}}\right)=\boldsymbol{\Omega}\times\left(L_e\frac{\boldsymbol{\xi}_e}{\boldsymbol{\xi}}\right)-\frac{1}{\tau_B}\frac{L_e}{\boldsymbol{\xi}_e}(\boldsymbol{\xi}_e-\boldsymbol{\xi})-\frac{{L_e}^2}{2\tau_B{\boldsymbol{\xi}_e}^3}\boldsymbol{\xi}_e\times(\boldsymbol{\xi}_e-\boldsymbol{\xi}). \tag{14}$$

The effective field can be expressed by the equation of zero approximation from the Eq. (14) as

$$\tau_B \frac{d\boldsymbol{\xi}_e}{dt} = -\left(\frac{d\ \log \boldsymbol{L}_e}{d\boldsymbol{\xi}_e}\right)^{-1}\left(1-\frac{\boldsymbol{\xi}_o}{\boldsymbol{\xi}_e}\ \cos\omega_o t\right). \tag{15}$$

Above, the parameters ω_o and ξ_o are frequency and amplitude of the real magnetic field, whereas the effective Langevin function is donated as parameter L_e is, of the field. From [33], using linear approximations in $\boldsymbol{\Omega}\tau_B$ and the expression

$$\boldsymbol{M}^{(1)} = \boldsymbol{M}^{(0)} R(\xi_e)\tau_B\, \boldsymbol{\Omega}\times\boldsymbol{h}, \tag{16}$$

where $\boldsymbol{M}^{(0)} = \phi \boldsymbol{M}_s \boldsymbol{L}(\boldsymbol{\xi})$ and $\boldsymbol{h}$ is unit vector along the applied field, Eq. (14) reduces to

$$\tau_B \frac{dR(\boldsymbol{\xi}_e)}{dt} = \left(1-\frac{1}{2}\left(\frac{1}{\boldsymbol{L}_e}-\frac{1}{\boldsymbol{\xi}_e}\right)\boldsymbol{\xi}_o R(\boldsymbol{\xi}_e)\ \cos\omega_0 t\right). \tag{17}$$

Since magnetic torque is not equal to zero, so from Eqs. (12) and (17), the expression for mean magnetic torque becomes

$$\overline{\boldsymbol{M}\times\boldsymbol{H}} = -6\mu\phi\,\boldsymbol{\Omega} g,\ g = \frac{1}{2}\boldsymbol{\xi}_0\,\overline{\cos\omega_0 t \boldsymbol{L}(\boldsymbol{\xi}_e)R(\boldsymbol{\xi}_e)}. \tag{18}$$

Here, $g(\xi_0, \omega_0\tau_B)$ is the effective magnetization parameter.

$$\frac{1}{2}\boldsymbol{\nabla}\times\overline{\boldsymbol{M}\times\boldsymbol{H}} = \frac{1}{2}\boldsymbol{\nabla}\times -6\mu_f\phi g\boldsymbol{\Omega} = -\frac{3}{2}\mu_f\phi g\boldsymbol{\nabla}(\boldsymbol{\nabla}.\mathbf{V}) = \frac{3}{2}\mu_f\phi g\nabla^2\mathbf{V}. \tag{19}$$

In view of Eqs. (19), (10) takes the following form

$$\rho_{nf}\frac{d\mathbf{V}}{dt} = -\boldsymbol{\nabla}p + (\boldsymbol{M}.\boldsymbol{\nabla})\boldsymbol{H} + \left(\mu_{nf}+\frac{3}{2}\mu_f\phi g\right)\nabla^2\mathbf{V}, \tag{20}$$

$$\rho\frac{d\mathbf{V}}{dt} = -\boldsymbol{\nabla}\tilde{p} + \left(\mu_{nf}+\frac{3}{2}\mu_f\phi g\right)\nabla^2\mathbf{V}. \tag{21}$$

As $-\boldsymbol{\nabla}\tilde{p} = -\boldsymbol{\nabla}p + (\boldsymbol{M}.\boldsymbol{\nabla})\boldsymbol{H}$ i.e., reduced pressure and equations of continuity, motion and temperature in cylindrical form subject to the boundary conditions can be written as

$$\frac{\partial v_r}{\partial r}+\frac{v_r}{r}+\frac{\partial v_z}{\partial z} = 0, \tag{22}$$

$$-\frac{\partial\tilde{p}}{\partial r}+\left(\mu_{nf}+\frac{3}{2}\mu_f\phi g\right)\left[\frac{\partial^2 v_r}{\partial r^2}+\frac{\partial}{\partial r}\left(\frac{v_r}{r}\right)+\frac{\partial^2 v_r}{\partial z^2}\right] = \rho_{nf}\left[\frac{\partial v_r}{\partial t}+v_r\frac{\partial v_r}{\partial r}+v_z\frac{\partial v_r}{\partial z}-\frac{v_\theta^2}{r}\right], \tag{23}$$

$$\left(\mu_{nf}+\frac{3}{2}\mu_f\phi g\right)\left[\frac{\partial^2 v_\theta}{\partial r^2}+\frac{\partial}{\partial r}\left(\frac{v_\theta}{r}\right)+\frac{\partial^2 v_\theta}{\partial z^2}\right] = \rho_{nf}\left[\frac{\partial v_\theta}{\partial t}+v_r\frac{\partial v_\theta}{\partial r}+v_z\frac{\partial v_\theta}{\partial z}+\frac{v_r v_\theta}{r}\right], \tag{24}$$

$$-\frac{\partial\tilde{p}}{\partial z}+\left(\mu_{nf}+\frac{3}{2}\mu_f\phi g\right)\left[\frac{\partial^2 v_z}{\partial r^2}+\frac{1}{r}\frac{\partial v_z}{\partial r}+\frac{\partial^2 v_z}{\partial z^2}\right] = \rho_{nf}\left[\frac{\partial v_z}{\partial t}+v_r\frac{\partial v_z}{\partial r}+v_z\frac{\partial v_z}{\partial z}\right], \tag{25}$$

$$(\rho C_p)_{nf}\left[\frac{\partial T}{\partial t}+v_r\frac{\partial T}{\partial r}+v_z\frac{\partial T}{\partial z}\right] = k_{nf}\left[\frac{\partial^2 T}{\partial r^2}+\frac{1}{r}\frac{\partial T}{\partial r}+\frac{\partial^2 T}{\partial z^2}\right], \tag{26}$$

$$\left.\begin{array}{l} at\ z=0;\quad v_r=\dfrac{\alpha\Omega_v r}{1-\beta t},\ v_\theta=\dfrac{\Omega_v r}{1-\beta t},\ v_z=0,\ T(r,\theta,z)=T_w \\ at\ z=\infty;\quad v_r=0,\ v_\theta=0,\ T(r,\theta,z)=T_\infty \end{array}\right\}. \tag{27}$$

Utilizing the following transformations

$$\left.\begin{array}{l} \eta=\sqrt{\dfrac{\Omega}{\nu_f}}\dfrac{z}{\sqrt{1-\beta t}},\ v_r(r,\theta,z)=\dfrac{\Omega r}{1-\beta t}F(\eta), v_\theta(r,\theta,z)=\dfrac{\Omega r}{1-\beta t}G(\eta), \\ v_z(r,\theta,z)=\sqrt{\dfrac{\Omega\nu_f}{1-\beta t}}E(\eta),\ \ \theta(\eta)=\dfrac{T-T_\infty}{T_w-T_\infty}, \dfrac{p}{\rho_f}=-\dfrac{\Omega\nu_f}{1-\beta^* t}\mathrm{P}(\eta) \end{array}\right\}. \tag{28}$$

into Eqs. (22) to (26), the dimensionless nonlinear system of ordinary differential equations along with the associated boundary connotation take the following form:

$$2F(\eta)+E'(\eta) = 0, \tag{29}$$

$$\frac{\rho_{nf}}{\rho_f}\left[F^2-G^2+EF'+S\left(F+\frac{\eta}{2}F'\right)\right] = \left(\frac{\mu_{nf}}{\mu_f}+\frac{3}{2}\phi g\right)F'', \tag{30}$$

$$\frac{\rho_{nf}}{\rho_f}\left[EG'+2FG+S\left(G+\frac{\eta}{2}G'\right)\right] = \left(\frac{\mu_{nf}}{\mu_f}+\frac{3}{2}\phi g\right)G'', \tag{31}$$

$$\frac{\rho_{nf}}{\rho_f}\left[EE'+\frac{S}{2}(E+\eta E')\right] = -\frac{\partial P}{\partial\eta}+\left(\frac{\mu_{nf}}{\mu_f}+\frac{3}{2}\phi g\right)E'', \tag{32}$$

$$\frac{(\rho C_p)_{nf}}{(\rho C_p)_f}\ \mathrm{Pr}\left[E\theta'+S\frac{\eta}{2}\theta'\right] = \frac{k_{nf}}{k_f}\theta'', \tag{33}$$

$$\left.\begin{array}{l} F(0)=\alpha,\quad G(0)=1,\quad E(0)=0,\ \ \theta(0)=1, \\ F(\infty)=0,\quad G(\infty)=0,\quad \theta(\infty)=0 \end{array}\right\}. \tag{34}$$

where, $\mathrm{Pr}=\frac{\mu_f C_{p\,f}}{k_f}$ is modified Prandtl number and $S=\frac{\beta}{\Omega_v}$ is the unsteadiness parameter.

3. Solutions of the problem

In section emphasis will be given to determine analytical solutions for velocity, temperature and nano-concentration distributions by using the following models:

3.1. Nano-ferroliquid models

The effective density ρ_{nf}, heat capacitance$(C_p)_{nf}$, viscosity μ_{nf}, and thermal conductive k_{nf} for nano-ferroliquid as given in Eqs. (22) to (26), are defined by

$$\rho_{nf} = (1-\phi_a)\rho_f+\phi\rho_a, \tag{35}$$

$$(\rho C_p)_{nf} = (1-\phi_a)(\rho C_p)_f+\phi_a(\rho C_p)_a, \tag{36}$$

$$k_{nf} = \frac{k_a+2k_f+2\phi_a(k_a-k_f)}{k_a+2k_f-\phi_a(k_a-k_f)}k_f, \tag{37}$$

$$\mu_{nf} = \mu_f\left(1-\frac{\phi_a}{\phi_{\max}}\right)^{-2.5\phi_{\max}}. \tag{38}$$

The subscripts a and f illustrates to aggregate and base liquid water. Further, the thermal properties of particle aggregation are given as

$$\rho_a = (1-\phi_{\mathrm{int}})\rho_f+\phi_{\mathrm{int}}\rho_s, \tag{39}$$

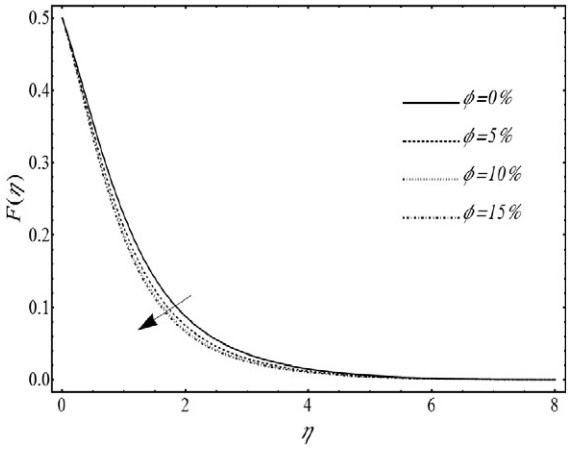

Fig. 2. Radial velocity profile corresponding to various values of nanoparticle volume fraction.

$$(C_p)_a = (1-\phi_{\text{int}})(C_p)_f + \phi_{\text{int}}(C_p)_s. \tag{40}$$

Above subscript s is used for solid single particle. The ϕ_{int} is donated for the nanoparticles volume fraction in cluster or in aggregate and $\phi = \phi_{\text{int}}\phi_a$. With the influence of magnetics particles become lineup in direction of filed that make a chain which call backbone and other particles that are free are called dead-end particles. In this situation, thermal conductivity is combination of backbone and dead-end particles thermal conductivities. The effective thermal conductivity of dead-end particles is given as

$$(1-\phi_{nc})(k_f-k_{nc})/(k_f+2k_m) + \phi_{nc}(k_s-k_{nc})/(k_s+2k_{nc}) = 0. \tag{41}$$

The thermal conductivity of aggregate k_a is determined by using composite theory for misoriented ellipsoidal particles for the backbone, the following equations are used

$$k_a = k_{nc}\frac{3+\phi_c[2\beta_{11}(1-L_{11})+\beta_{33}(1-L_{33})]}{3-\phi_c[2\beta_{11}L_{11}+\beta_{33}L_{33}]}, \tag{42}$$

where

$$\left.\begin{array}{l} L_{11} = 0.5p^2/(p^2-1) - 0.5p\cosh^{-1}p/(p^2-1)^{1.5}, \\ L_{33} = 1-2L_{11}, \\ \beta_{ii} = (k_{ii}^c-k_{nc})/[k_{nc}-L_{ii}(k_{ii}^c-k_{nc})] \end{array}\right\}. \tag{43}$$

Interfacial resistance is accounted for in the term

$$k_{ii}^c = k_s/(1+\gamma L_{ii}k_s/k_f). \tag{44}$$

Here $\gamma = (2+1/p)\alpha, \alpha = A_k/a_1$, $A_k$is the kapitza radius and $p = R_g a_1$. The number of particles in aggregation and in belonging to backbone are calculated through

$$N_{\text{int}} = (R_g/a_1)^{d_f}, \tag{45}$$

$$N_c = (R_g/a_1)^{d_l}. \tag{46}$$

where a_1 is the radius of the primary particle, R_g is average radius of gyration, d_f is fractal dimensions and d_l is chemical dimension.

The volume fraction of backbone particles ϕ_c and particles belonging to dead ends ϕ_{nc} is given by

$$\phi_c = (R_g/a_1)^{d_l-3}. \tag{47}$$

$$\phi_{nc} = \phi_{\text{int}} - \phi_c, \tag{48}$$

where $\phi_{\text{int}} = (R_g/a_1)^{1/d_f-3}$.

3.2. Skin friction coefficient and Nusselt number

The skin fraction coefficient C_f and the Nusselt number Nu are physical quantities which are given by

$$C_f = \frac{\sqrt{\tau_{wr}^2+\tau_{w\phi}^2}}{\rho_f\left(\frac{\alpha\Omega r}{1-\beta t}\right)^2}, \quad Nu = \frac{rq_w}{k_f(T_w-T_\infty)}. \tag{49}$$

where τ_{wr} and $\tau_{w\phi}$ are the radial and the transversal skin fraction or shear stress at the surface of disk, respectively, and q_w is the surface heat flux, introduced as

$$\tau_{wr} = \left(\mu_{nf}+\frac{3}{2}\mu_f\phi g\right)\left(\frac{\partial v_r}{\partial z}+\frac{\partial v_z}{\partial \theta}\right)_{z=0}, \quad \tau_{w\phi} = \left(\mu_{nf}+\frac{3}{2}\mu_f\phi g\right)\left(\frac{\partial v_\theta}{\partial z}+\frac{1}{r}\frac{\partial v_z}{\partial \theta}\right)_{z=0}, \quad q_w = -k_{nf}(T_z)_{z=0}. \tag{50}$$

After substituting Eqs. (28) and (50) in Eq. (49), we have

$$\text{Re}^{\frac{1}{2}}C_f = \left(\frac{\mu_{nf}}{\mu_f}+\frac{3}{2}\phi g\right)\sqrt{F'(0)^2+G'(0)^2}, \quad \text{Re}^{-\frac{1}{2}}Nu = -\frac{k_{nf}}{k_f}\theta'(0). \tag{51}$$

Here $\text{Re} = \Omega_v r^2/\nu_f(1-\beta t)$ is the rotational Reynolds number.

3.3. Boundary layer displacement thickness

Thickness of boundary layer can be found by finding the separation over inertia and viscous forces are practically identical. The velocity in the boundary layer accomplishes a value which is near the external velocity as of now at a little separation from the wall. The boundary layer displacement thickness is ascertained as

$$d = \frac{1-\beta t}{\Omega r}\int_{z=0}^{\infty} v_\theta dz = r\text{Re}^{-1/2}\int_{\eta=0}^{\infty} G(\eta)d\eta. \tag{52}$$

3.4. Outward flowing volume and rotation angle of liquid

Total volume flowing outward the z-axis,

$$Q = 2\pi r\int_0^{\infty} v_r dz = 2\pi r\nu_f \text{Re}^{1/2}\int_0^{\infty} F(\eta)d\eta. \tag{53}$$

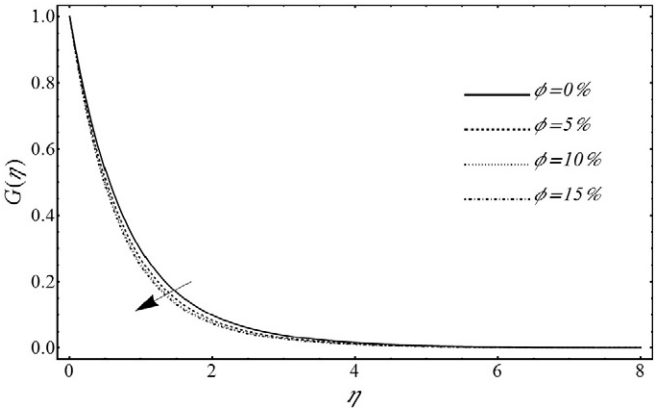

Fig. 3. Tangential velocity profile corresponding to various values of nanoparticle volume fraction.

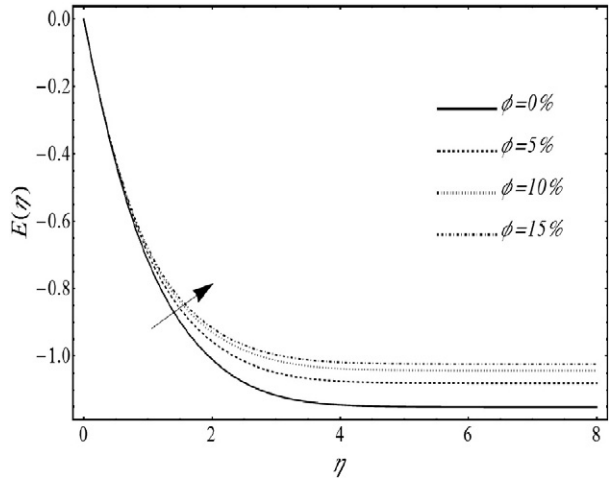

Fig. 4. Axial velocity profile corresponding to various values of nanoparticle volume fraction.

The liquid is taken to rotate at a large distance from the wall, the angle becomes

$$\tan(\psi_0) = -\left(\frac{\partial v_r}{\partial v_z} \Big/ \frac{\partial v_\theta}{\partial v_z}\right) = -\frac{F'(\eta)}{G'(\eta)} = -10.67 = -84.6^o. \tag{54}$$

3.5. Homotopic method

Due to nonlinear nature of Eqs. (29)–(33), an exact solution is not possible. Now, we opted to go for analytic solution. In order to serve the purpose HAM based package BVPh 2.0 is employed for solving nonlinear differential equation using computational software Mathematica 9. In this package, it is needed to put appropriate initial guess of solutions and auxiliary linear operators to find the desire solution which are given as

$$\left.\begin{aligned} &\pounds_E(H) = \frac{dE}{d\eta}, \quad \pounds_F(F) = \frac{dF}{d\eta} + \frac{d^2F}{d\eta^2}, \\ &\pounds_G(G) = \frac{dG}{d\eta} + \frac{d^2G}{d\eta^2}, \quad \pounds_\theta(\theta) = 2\frac{d\theta}{d\eta} + \frac{d^2\theta}{d\eta^2}, \end{aligned}\right\} \tag{55}$$

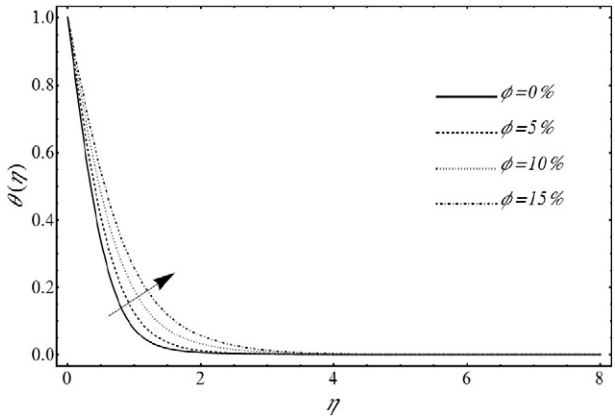

Fig. 5. Temperature profile corresponding to various values of nanoparticle volume fraction.

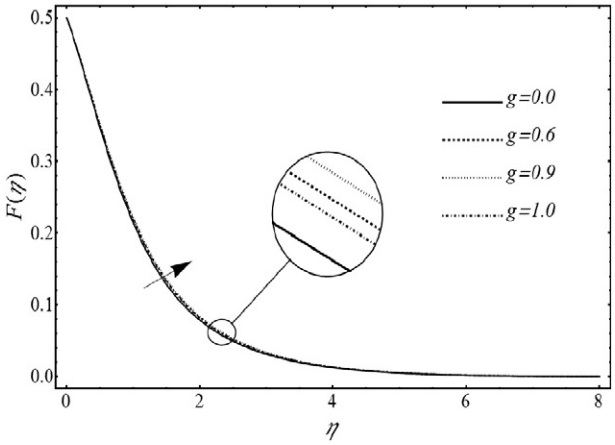

Fig. 6. Radial velocity profile corresponding to various values of effective magnetization parameter.

$$\left.\begin{aligned} &E_o = 0, \quad F_o(\eta) = \alpha e^{-\eta}, \\ &G_o(\eta) = e^{-\eta}, \quad \theta_o(\eta) = e^{-2\eta} \end{aligned}\right\}, \tag{56}$$

Thus the analytical expressions for velocity, temperature and concentrations up to first iteration are obtained as follows:

$$\begin{aligned} F = &\left(\frac{1}{2} + \frac{83}{400}\left(\frac{\mu_{nf}}{\mu_f} + \frac{3}{2}\phi g\right) + \frac{83}{800}\left(\frac{\rho_{nf}}{\rho_f}\right) - \right. \\ &\left. \frac{83S}{1600}\left(\frac{\rho_{nf}}{\rho_f}\right) - \frac{249}{800}\left(\frac{\mu_{nf}}{\mu_f} + \frac{3}{2}\phi g\right)\right) e^{-z} \\ &+ \left(\frac{-83}{400}\left(\frac{\mu_{nf}}{\mu_f}\right) + \frac{83S}{1600}\left(\frac{\rho_{nf}}{\rho_f}\right) - \right. \\ &\left. \frac{83S}{800}\left(\frac{\rho_{nf}}{\rho_f}\right)z - \frac{249}{800}\left(\frac{\mu_{nf}}{\mu_f} + \frac{3}{2}\phi g\right)\right) e^{-2z} - \left(\frac{83}{800}\left(\frac{\rho_{nf}}{\rho_f}\right)\right) e^{-3z}, \end{aligned} \tag{61}$$

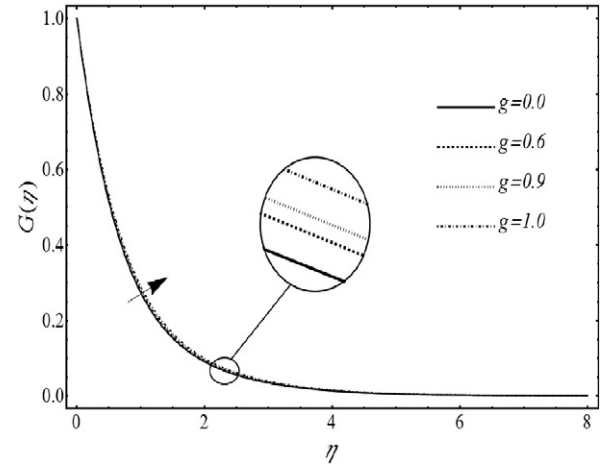

Fig. 7. Tangential velocity profile corresponding to various values of effective magnetization parameter.

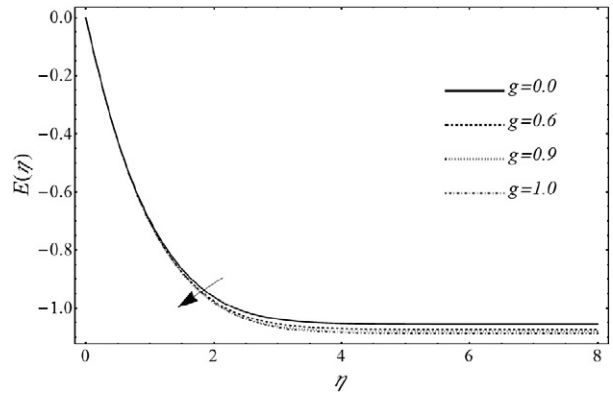

Fig. 8. Axial velocity profile corresponding to various values of effective magnetization parameter.

$$G=\left(1+\frac{43}{200}\left(\frac{\mu_{nf}}{\mu_f}\right)-\frac{43}{600}\left(\frac{\rho_{nf}}{\rho_f}\right)-\frac{43S}{800}\left(\frac{\rho_{nf}}{\rho_f}\right)+\frac{192}{400}\left(\frac{\mu_{nf}}{\mu_f}+\frac{3}{2}\phi g\right)\right)e^{-z}+\left(-\frac{43}{200}\left(\frac{\mu_{nf}}{\mu_f}\right)+\frac{43S}{800}\left(\frac{\rho_{nf}}{\rho_f}\right)-\frac{43S}{400}\left(\frac{\rho_{nf}}{\rho_f}\right)z-\frac{192}{400}\left(\frac{\mu_{nf}}{\mu_f}+\frac{3}{2}\phi g\right)\right)e^{-2z}-\left(\frac{43}{600}\left(\frac{\rho_{nf}}{\rho_f}\right)\right)e^{-3z}, \tag{62}$$

$$E=e^{-2z}\left(-\frac{73}{100}+\frac{73}{100}\right), \tag{63}$$

$$T=\left(-\frac{53}{75}\left(\frac{k_{nf}}{k_f}\right)-\frac{53}{225}\,\mathrm{Pr}S-\frac{53}{300}\,\mathrm{Pr}S\left(\frac{(\rho C_p)_{nf}}{(\rho C_p)_f}\right)z\right)e^{-3z}+\left(1+\frac{53}{75}\left(\frac{k_{nf}}{k_f}\right)+\frac{53}{225}\,\mathrm{Pr}S\left(\frac{(\rho C_p)_{nf}}{(\rho C_p)_f}\right)\right)e^{-2z}. \tag{64}$$

4. Results and discussion

In this section the behavior of emerging parameters involved in the expression of velocity and temperature distributions are examined through Figs. 2 to 9 with water based nano-ferroliquid contained Iron nanoparticles in water with low isolating magnetic field effect are taken to account. The radius of gyration is considered 200 nm while each sphere shape particles has 10*nm* radius. In single aggregation, the total particles are 200 in which 50 particles belong to backbone. The value of stretching parameter is chosen $\alpha=0.5$ and unsteadiness parameter is selected $S=0.5$ in order to see the behavior of particles concentration and magnetization effects on velocity and temperature profiles. Figs. 2 to 4, represent radial, tangential and axial velocity profiles for different value of particle concentration against a dimensionless parameter η. In these figures, it is noticed that several velocity lines have been publicized corresponding to different concentration of nanoparticles. By diverse concentration, unalike collisions between neighboring particles in a liquid are produced different velocity lines. It is also noticed that when the nanoparticle concentration is enhanced, all velocity components are declined. This is accordance with the physical expectation because heighten of resistance between adjacent layers of moving liquid. Therefore, the base liquid has much velocity as compared to ferroliquid. Fig. 5, shows the effect of particle concentrations on temperature profile. It is seen that the temperature of nanoliquid is enhanced by cumulative of nanoparticles volume fraction. The improvement in thermal conduction of the liquid due to magnetic particles makes a cause of enhancement in temperature. Figs. 6–8, characterize the radial, tangential and axial velocities profiles for various values of effective magnetization parameter. It is seen that magnetization parameter has no so much influence on velocity in different directions. When low oscillating magnetic field is applied on liquid then means angular velocity of the particles become less than to angular velocity of liquid. That why, magnetization parameter effects are not so dominant. It is also seen that when effective magnetization parameter is declined, the all velocity components are little bit decreased. This is due to increasing in angular velocity of the particle which leads to declination in magnetization influences and produced an additional resistance in ferroliquid. Fig. 9, shows the effect of magnetization parameter on temperature profile. It is seen that the temperature is amplified by boosting the influence of magnetization parameter. The consequence of magnetization parameter indicates the enhancement in rotational viscosity that becomes cause of enrichment of temperature. The numerical sets of values show the results for parameters of physical interest. The impact of particle volume fraction on skin-friction coefficient, local Nusselt, boundary layer thickness and volume flowing outward the *z*-axis are shown in Table 1. Skin friction arises when the liquid has interaction with the surface of the body. It is seen that when nanoparticle volume fraction enhances shear stress at wall is increased. The shear stress depends on the dynamic viscosity and the acceleration. it is found that when particle concentration is increased, the gradient of the velocity and dynamic viscosity increases that are caused in enhancement in shear stress at wall. In Table 1, it is observed that when nanoparticle volume fraction

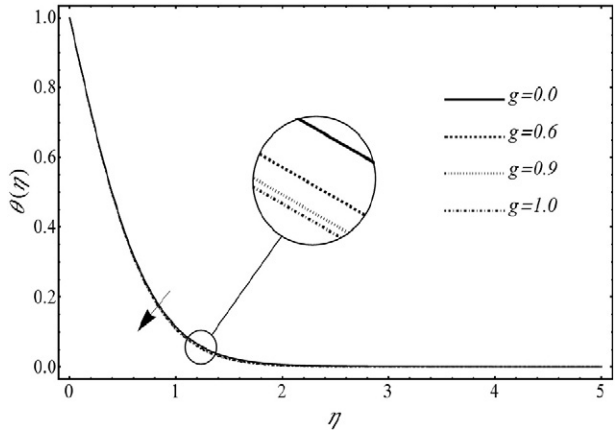

Fig. 9. Temperature profile corresponding to various values of effective magnetization parameter.

Table 1
Values of skin-friction coefficient, local Nusselt, boundary layer thickness, volume flowing outward the z-axis and angle corresponding to various values of nanoparticle volume fraction.

$\mathrm{Re}^{1/2}N_u\phi$	$\mathrm{Re}^{1/2}C_f s$	$\mathrm{Re}^{1/2}Nu$	d	Q
0%	1.2625	1.5851	0.8579	0.6026
5%	1.5883	1.7171	0.8056	0.5669
10%	1.9313	1.8246	0.7813	0.5502
15%	2.2949	1.9412	0.7719	0.5436

Table 2
Values of skin-friction coefficient, local Nusselt, boundary layer thickness, volume flowing outward the z-axis and angle corresponding to various values of effective magnetization parameter.

$\mathrm{Re}^{1/2}N_u g$	$\mathrm{Re}^{1/2}C_f$	$\mathrm{Re}^{1/2}Nu$	d	Q
0	1.5629	1.7097	0.7934	0.5585
0.6	1.5933	1.7182	0.8101	0.5699
0.9	1.6084	1.7225	0.8153	0.5735
1	1.6134	1.7235	0.8177	0.5752

Table 3
Comparison of the obtained results for the values of $F'(0)$ and $G'(0)$ when $\phi = 0\%$ and $g = 0$.

	$F'(0)$		$G'(0)$	
S	Present	Rashidi [34]	Present	Rashidi [34]
−0.1	−3.1187	−3.1178	−2.0532	−2.0530
−0.5	−2.9632	−2.9601	−1.9907	−1.9901
−1	−2.7621	−2.7622	−1.9204	−1.9111

enhances, heat transfer rate at wall increases. Thermal conductivity of liquid plays an important role in the heat transfer rate. For example, enhancement in thermal conductivity of liquid is found 25.12% and 54.81% at 5% and 10% concentration of nanoparticles. Then with same trend, enhancement in heat transfer rate at wall is found 8.33% and 15.11% at 5% and 10% concentrations. Boundary layer displacement describes the difference between the case with boundary layer flow over a surface and the actual flow without a boundary layer. It is noticed that boundary layer displacement decreases corresponding to concentration of particle. Furthermore, the total volume flowing outward the z-axis is decreased as increasing of particles concentrations. In Table 2, the result of effective magnetization parameter on skin-friction coefficient, local Nusselt, boundary layer thickness and volume flowing outward the z-axis is publicized. It is perceived that with augmentation of magnetization parameter declines, there the shear stress and heat transfer rate at the wall. In the other sundry parameters, displacement thickness is increased because of enrichment in boundary layer thickness due to consequences of magnetization parameter. Furthermore, the total volume flowing outward the z-axis is also increased. The obtained results have also been compared with the existing literature [34] as shown in Table 3 and are found in good agreement which offers a useful check that the reported results are correct and also provides a clear reliance on presented mathematical description.

5. Concluding remarks

In this paper, unsteady ferroliquid flow revolving a stretchable rotating disk on a boundary layer is presented. It is observed that enhancement of ferro-particles concentration changes the physical properties of liquid which distresses the liquid velocity and temperature distribution. The axial velocity component is maximum affect than the redial velocity component and much more than the tangential velocity component under effects of particles concentrations. The velocity of liquid is declined due to increasing of resistance between layers by particles concentrations. Moreover, the temperature of liquid is heightened due to enhancement in thermal conductivity by magnetic particles. It has been found that velocity components are not highly affected by magnetization as compare to particles concentration effects. But in velocity components, axial velocity due to magnetization is dominant in comparison to the radial and tangential velocity. The magnetization amplifies and diminishes to velocity and temperature profiles. From numerical results, it is seen that shear stress at wall is vastly increased when concentration improved and slowly decreased due to magnetization effect. Heat transfer rate at wall in ferroliquid is much improved in comparison of water. Magnetization is also play a role to improve heat transfer rate at wall but not as concentration. The fluctuating in displacement thickness and outward volume flow has same behavior as velocity under both effects.

References

[1] R.E. Rosensweig, Ferrohydrodynamics, Cambridge University Press, Cambridge, England, 1985.
[2] P. Ram, A. Bhandari, K. Sharma, Effect of magnetic field-dependent viscosity on revolving ferrofluid, J. Magn. Magn. Mater. 322 (2010) 3476–3480.
[3] P.D.S. Verma, P. Ram, On the low-Reynolds number magnetic fluid flow in a helical pipe, Int. J. Eng. Sci. 31 (1993) 229–239.
[4] S. Odenbach, Magnetic fluids, Adv. Colloid Interf. Sci. 46 (1993) 263–282.
[5] K. Milani Shirvan, M. Mamourian, S. Mirzakhanlari, R. Ellahi, Two phase simulation and sensitivity analysis of effective parameters on combined heat transfer and pressure drop in a solar heat exchanger filled with nanofluid by RSM, J. Mol. Liq. 220 (2016) 888–901.
[6] M. Akbarzadeh, S. Rashidi, M. Bovand, R. Ellahi, A sensitivity analysis on thermal and pumping power for the flow of nanofluid inside a wavy channel, J. Mol. Liq. 220 (2016) 1–13.
[7] A. Zeeshan, A. Majeed, R. Ellahi, Effect of magnetic dipole on viscous ferro-fluid past a stretching surface with thermal radiation, J. Mol. Liq. 215 (2016) 549–554.
[8] M. Sheikholeslami, R. Ellahi, Simulation of ferrofluid flow for magnetic drug targeting using lattice Boltzmann method, J. Z. Naturforsch. A 70 (2015) 115–124.
[9] O. Mahian, A. Kianifar, S.A. Kalogirou, I. Pop, S. Wongwises, A review of the applications of nanofluids in solar energy, Int. J. Heat Mass Transf. 57 (2013) 582–594.
[10] S. Ahmad, A.M. Rohni, I. Pop, Blasius and sakiadis problems in nanofluids, Acta Mech. 218 (2011) 195–204.
[11] S.T. Mohyud-Din, Z.A. Zaidi, U. Khan, N. Ahmed, On heat and mass transfer analysis for the flow of a nanofluid between rotating parallel plates, Aerosp. Sci. Technol. 46 (2015) 514–522.
[12] R. Ellahi, S.U. Rahman, S. Nadeem, Blood flow of Jeffrey fluid in a catherized tapered artery with the suspension of nanoparticles, Phys. Lett. A 378 (2014) 2973–2980.
[13] N. Shahzad, A. Zeeshan, R. Ellahi, K. Vafai, Convective heat transfer of nanofluid in a wavy channel: Buongiorno's mathematical model, J. Mol. Liq. 222 (2016) 446–455.
[14] A. Zeeshan, A. Majeed, R. Ellahi, Unsteady ferromagnetic liquid flow and heat transfer analysis over a stretching sheet with the effect of dipole and prescribed heat flux, J. Mol. Liq. 223 (2016) 528–533.
[15] M.M. Bhatti, M.M. Rashidi, Effects of thermo-diffusion and thermal radiation on Williamson nanofluid over a porous shrinking/stretching sheet, J. Mol. Liq. 221 (2016) 567–573.
[16] A. Engel, H.W. Muller, P. Reimann, A. Jung, Ferrofluids as thermal ratchets, Phys. Rev. Lett. 91 (2003) 060602–060606.
[17] M.I. Shliomis, K.I. Morozov, Negative viscosity of ferrofluid under alternating magnetic field, Phys. Fluids 6 (1994) 2855–2861.
[18] M.M. Bhatti, R. Ellahi, A. Zeeshan, Study of variable magnetic field on the peristaltic flow of Jeffrey fluid in a non-uniform rectangular duct having compliant walls, J. Mol. Liq. 222 (2016) 101–108.
[19] M.D. Gupta, A.S. Gupta, Convective instability of a layer of a ferromagnetic fluid rotating about a vertical axis, Int. J. Eng. Sci. 17 (1979) 271–277.
[20] G. Vaidyanathan, R. Sekar, A. Ramanathan, Effect of magnetic field dependent viscosity on ferroconvection in a rotating medium, Indian J. Pure Appl. Phys. 40 (2002) 159–165.
[21] A. Ramanathan, G. Suresh, Effect of magnetic field dependent viscosity and anisotropy of porous medium on ferroconvection, Int. J. Eng. Sci. 42 (2004) 411–425.
[22] P. Ram, K. Sharma, Effect of rotation and MFD viscosity on ferrofluid flow with rotating disk, Indian J. Pure Appl. Phys. 52 (2014) 87–92.
[23] P. Ram, V. Kumar, S. Sharma, Magneto-viscous effects on unsteady nano-ferrofluid flow influenced by low oscillating magnetic field in the presence of rotating disk, Recent Advances in Fluid Mechanics and Thermal Engineering 2014, pp. 89–97.
[24] S.J. Liao, The Proposed Homotopy Analysis Technique for the Solution of Nonlinear Problems(Ph.D. dissertation) Shanghai Jiao Tong University, Shanghai China, 1992.
[25] Y. Zhao, S.J. Liao, HAM-Based Package BVPh 2.0 for Nonlinear Boundary Value Problems, in: S. Liao (Ed.), Advances in Homotopy Analysis Method, World Scientific Press, 2013.
[26] R. Ellahi, M. Hassan, A. Zeeshan, Aggregation effects on water base Al_2O_3 − nanofluid over permeable wedge in mixed convection, Asia Pac. J. Chem. Eng. 11 (2016) 179–186.
[27] R. Ellahi, S. Aziz, A. Zeeshan, Non-Newtonian fluid flow through a porous medium between two coaxial cylinders with heat transfer and variable viscosity, J. Porous Media 16 (2013) 205–216.
[28] E. Blums, A. Cebers, M.M. Maiorov, Magnetic Fluids, Walter de Gruyter, Berlin and New York, 1997.
[29] R.E. Rosensweig, Ferrohydrodynamics, Cambridge University Press, 1985.
[30] M.I. Shliomis, K.I. Morozov, Negative viscosity of ferrofluid under alternating magnetic field, Phys. Fluids 6 (1940) 2855–2861.
[31] P. Ram, A. Bhandari, Negative viscosity effects on ferrofluid flow due to a rotating disk, Int. J. Appl. Electromagn. Mech. 41 (2013) 467–478.
[32] M.I. Shliomis, Ferrohydrodynamics, testing a third magnetization equation, Phys. Rev. E 64 (2001) 060–501.
[33] H. Schlichting, Boundary Layer Theory, McGraw-Hill Book Company, New York, 1960.
[34] M.M. Rashidi, M. Ali, N. Freidoonimehr, F. Nazari, Parametric analysis and optimization of entropy generation in unsteady MHD flow over a stretching rotating disk using artificial neural network and particle swarm optimization algorithm, Energy 55 (2013) 497–510.